

LETTER TO THE EDITOR

# Direct Discovery of the Inner Exoplanet in the HD 206893 System Evidence for Deuterium Burning in a Planetary Mass Companion

S. Hinkley<sup>1</sup>, S. Lacour<sup>2,3</sup>, G.-D. Marleau<sup>4,5,6,7</sup>, A.-M. Lagrange<sup>8,2</sup>, J. J. Wang<sup>9</sup>, J. Kammerer<sup>10</sup>, A. Cumming<sup>32,33</sup>, M. Nowak<sup>11</sup>, L. Rodet<sup>12</sup>, T. Stolker<sup>14</sup>, W.-O. Balmer<sup>13,10</sup>, S. Ray<sup>1</sup>, M. Bonnefoy<sup>8</sup>, P. Mollière<sup>7</sup>, C. Lazzoni<sup>1</sup>, G. Kennedy<sup>15</sup>, C. Mordasini<sup>6</sup>, R. Abuter<sup>3</sup>, S. Aigrain<sup>31</sup>, A. Amorim<sup>16,17</sup>, R. Asensio-Torres<sup>7</sup>, C. Babusiaux<sup>8,2</sup>, M. Benisty<sup>8</sup>, J.-P. Berger<sup>8</sup>, H. Beust<sup>8</sup>, S. Blunt<sup>9</sup>, A. Boccaletti<sup>2</sup>, A. Bohn<sup>14</sup>, H. Bonnet<sup>3</sup>, G. Bourdarot<sup>18,8</sup>, W. Brandner<sup>7</sup>, F. Cantalloube<sup>19</sup>, P. Caselli<sup>18</sup>, B. Charnay<sup>2</sup>, G. Chauvin<sup>8</sup>, A. Chomez<sup>2,8</sup>, E. Choquet<sup>19</sup>, V. Christiaens<sup>20</sup>, Y. Clénet<sup>2</sup>, V. Coudé du Foresto<sup>2</sup>, A. Cridland<sup>14</sup>, P. Delorme<sup>8</sup>, R. Dembet<sup>2</sup>, P. T. de Zeeuw<sup>14,18</sup>, A. Drescher<sup>18</sup>, G. Duvert<sup>8</sup>, A. Eckart<sup>21,22</sup>, F. Eisenhauer<sup>18</sup>, H. Feuchtgruber<sup>18</sup>, F. Galland<sup>8</sup>, P. Garcia<sup>17,23</sup>, R. Garcia Lopez<sup>24,7</sup>, T. Gardner<sup>25</sup>, E. Gendron<sup>2</sup>, R. Genzel<sup>18</sup>, S. Gillessen<sup>18</sup>, J. H. Girard<sup>10</sup>, A. Grandjean<sup>8</sup>, X. Haubois<sup>26</sup>, G. Heißel<sup>235</sup>, Th. Henning<sup>7</sup>, S. Hippler<sup>7</sup>, M. Horrobin<sup>21</sup>, M. Houllé<sup>19</sup>, Z. Hubert<sup>8</sup>, L. Jocu<sup>8</sup>, M. Keppler<sup>7</sup>, P. Kervella<sup>2</sup>, L. Kreidberg<sup>7</sup>, V. Lapeyrière<sup>2</sup>, J.-B. Le Bouquin<sup>8</sup>, P. Léna<sup>2</sup>, D. Lutz<sup>18</sup>, A.-L. Maire<sup>8</sup>, F. Mang<sup>18</sup>, A. Mérand<sup>3</sup>, N. Meunier<sup>8</sup>, J. D. Monnier<sup>25</sup>, C. Mordasini<sup>6</sup>, D. Mouillet<sup>8</sup>, E. Nasedkin<sup>7</sup>, T. Ott<sup>18</sup>, G. P. L. Otten<sup>19,34</sup>, C. Paladini<sup>26</sup>, T. Paumard<sup>2</sup>, K. Perraut<sup>8</sup>, G. Perrin<sup>2</sup>, F. Philipot<sup>2</sup>, O. Pfuhl<sup>3</sup>, N. Pourré<sup>8</sup>, L. Pueyo<sup>10</sup>, J. Rameau<sup>8</sup>, E. Rickman<sup>27</sup>, P. Rubini<sup>26</sup>, Z. Rustamkulov<sup>28</sup>, M. Samland<sup>7</sup>, J. Shanguan<sup>18</sup>, T. Shimizu<sup>18</sup>, D. Sing<sup>13,28</sup>, C. Straubmeier<sup>21</sup>, E. Sturm<sup>18</sup>, L. J. Tacconi<sup>18</sup>, E.F. van Dishoeck<sup>14,18</sup>, A. Vigan<sup>19</sup>, F. Vincent<sup>2</sup>, K. Ward-Duong<sup>29</sup>, F. Widmann<sup>18</sup>, E. Wieprecht<sup>18</sup>, E. Wiezorrek<sup>18</sup>, J. Woillez<sup>3</sup>, S. Yazici<sup>18</sup>, A. Young<sup>18</sup>, N. Zicher<sup>30</sup>, and the GRAVITY Collaboration

(Affiliations can be found after the references)

Received XXXX; accepted XX XXX

## ABSTRACT

**Aims.** HD 206893 is a nearby debris disk star hosting a previously identified brown dwarf companion with a  $\sim 10$  au orbital separation. Long term precise radial velocity (RV) monitoring, as well as anomalies in the system proper motion, have suggested the presence of an additional, inner companion in the system. In this work we describe the results of a search for the companion responsible for this RV drift and proper motion anomaly.

**Methods.** Utilizing information from ongoing precision RV measurements with the HARPS spectrograph, as well as *Gaia* host star astrometry, we have undertaken a multi-epoch search for the purported additional planet using the VLT/GRAVITY instrument.

**Results.** We report a high significance detection of the purported companion HD 206893 c over three epochs, with clear evidence for Keplerian orbital motion. Our astrometry with  $\sim 50$ – $100$   $\mu$ sec precision afforded by GRAVITY allows us to derive a dynamical mass of  $12.3^{+1.1}_{-1.2} M_{\text{Jup}}$  and an orbital separation of  $3.53^{+0.08}_{-0.07}$  au for HD 206893 c. Our fits to the orbits of both companions in the system utilize both *Gaia* astrometry and RVs to also provide a precise dynamical estimate of the previously uncertain mass of the B component, and therefore derive an age of 170 Myr for the system. Importantly, we find that the bolometric luminosity of the newly discovered HD 206893 c is anomalously high, and that standard cooling curves are unable to simultaneously account for the brightness of both members of the system at a common age of 170 Myr. However, we find that incorporating an elevated helium abundance into our cooling models in turn results in an enhanced level of deuterium burning in HD 206893 c, bringing the predicted luminosity in line with our measured value.

**Conclusions.** In addition to utilizing long-term RV information, this effort is an early example of a direct imaging discovery of a bona fide exoplanet that was guided in part with *Gaia* astrometry. Utilizing *Gaia* astrometry is expected to be one of the primary techniques going forward to identify and characterize additional directly imaged planets. In addition, HD 206893 c is an example of an object narrowly straddling the deuterium-burning limit, likely undergoing deuterium burning, and making it an ideal laboratory to establish the precise mass where deuterium burning can occur. Additional discoveries like this may therefore help to clarify the discrimination between an object that would be considered a brown dwarf or an extrasolar planet. Lastly, this discovery is another example of the power of optical interferometry to directly detect and characterize extrasolar planets where they form at ice-line orbital separations of 2–3 au.

**Key words.** Planets and satellites: detection – Techniques: high angular resolution – Techniques: interferometric – Instrumentation: high angular resolution – Instrumentation: interferometers –

## 1. Introduction

What distinguishes an extrasolar giant planet (EGP) from a brown dwarf (BD) is still a matter of debate. The current IAU definition of a planet is an object that is below the mass required for thermonuclear fusion of deuterium, which we currently believe occurs at 13 Jupiter masses. Identifying objects near this

mass limit will clarify how distinct the boundary between massive planets and brown dwarfs really is (e.g., Mollière & Mordasini 2012; Bodenheimer et al. 2013). However, what qualifies an object to be an exoplanet may be more related to its formation mechanism rather than solely its mass (e.g., Chabrier et al. 2007). Hybrid exoplanetary systems containing both a brown

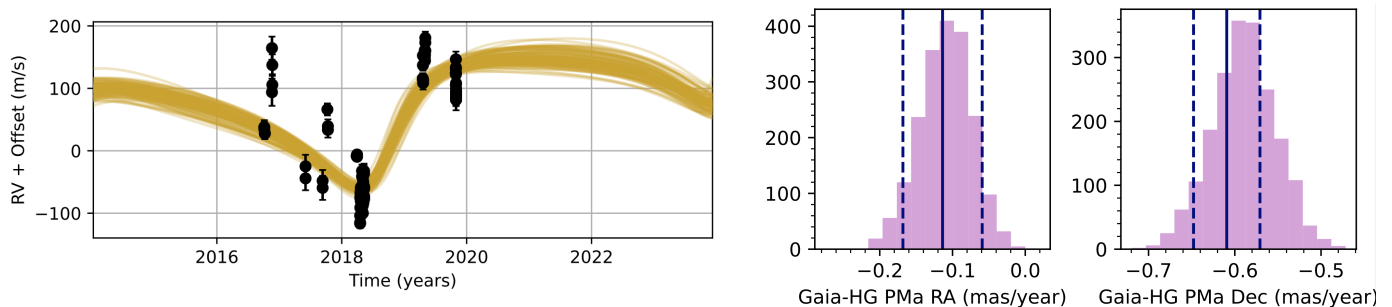


**Fig. 1.** *Left:* The HARPS radial velocities for HD 206893 (e.g. Grandjean et al. 2019a) along with samples from the posterior for the model fit to the radial velocities and Proper motion anomalies. *Right:* The posterior distributions for our best fit model of the predicted proper Motion Anomaly (purple histograms) calculated as the difference between the *Gaia* EDR2 proper motion and the long-term proper motion as calculated by comparing *Gaia* with *Hipparcos* (labelled “HG” in the figure) and displayed individually in terms of Right Ascension and Declination. The vertical blue lines show the actual values, with  $1\sigma$  uncertainties represented by the dashed lines.

dwarf as well as an exoplanet, which presumably formed at the same time from the same protoplanetary disk, are therefore ideal systems to study different possible formation pathways using diagnostics like atmospheric atomic ratios (e.g., Öberg et al. 2011; Madhusudhan et al. 2014; Mordasini et al. 2016; Mollière et al. 2022) or initial entropy (e.g., Spiegel & Burrows 2012; Marleau & Cumming 2014). Finding and characterizing planetary mass companions near this deuterium burning limit (e.g., Bowler et al. 2013; Bonnefoy et al. 2014; Hinkley et al. 2013), or systems containing both a brown dwarf and an exoplanet, will allow us to clarify how we draw a distinction between these two classes of objects (e.g., Mollière & Mordasini 2012).

HD 206893 is a nearby ( $40.707 \pm 0.067$  pc, Gaia Collaboration et al. 2018) F5V star with roughly solar metallicity ranging from  $[\text{Fe}/\text{H}] = -0.07$  to  $-0.05$  (Holmberg et al. 2007; Gáspár et al. 2016) to  $+0.01$  (Netopil 2017), and a highly uncertain age due to the lack of clear membership to any young kinematic moving groups. Most age estimates of this star have been in the range of 100–300 Myr (Zuckerman & Song 2004; Delorme et al. 2017; Milli et al. 2017; Kammerer et al. 2021), but some works have allowed ages as young as 3 or 50 Myr (Kammerer et al. 2021; Ward-Duong et al. 2021), while another has quoted an age as high as 2.1 Gyr (e.g., David & Hillenbrand 2015). A substellar companion, HD 206893 B was first identified in Milli et al. (2017) showing a projected orbital separation of  $\sim 10$  au using the VLT SPHERE instrument. The somewhat uncertain system age allowed only loose constraints on the mass of HD 206893 B, initially placing it in the range of  $24\text{--}73 M_{\text{Jup}}$  (Milli et al. 2017), but later refined to be as low as  $\sim 5 M_{\text{Jup}}$  (Kammerer et al. 2021) and up to  $30\text{--}40 M_{\text{Jup}}$  (Delorme et al. 2017; Kammerer et al. 2021; Ward-Duong et al. 2021). A careful estimation of the age of this system is thus absolutely critical for its full characterization. This object possesses extraordinarily red infrared colors, and has been characterized in numerous subsequent works (Delorme et al. 2017; Stolker et al. 2020; Meshkat et al. 2021; Ward-Duong et al. 2021; Kammerer et al. 2021).

Evidence has been emerging for an additional, inner companion in the system. Using precise radial velocity (RV) monitoring with the *HARPS* spectrograph over 1.6 yr, Grandjean et al. (2019a) revealed a significant RV drift that could not be solely due to HD 206893 B, and hypothesize the presence of a  $\sim 15 M_{\text{Jup}}$  companion. Similarly, Kammerer et al. (2021) showed that the anomaly in the *Gaia* EDR3 proper motion cannot be explained by the B companion alone, and constrain the parameter space spanned by the mass and on-sky position of an additional, hypothesized  $8\text{--}15 M_{\text{Jup}}$  companion.

In this paper, using optical interferometry over several epochs, we present the discovery of HD 206893 c, a  $\sim 12 M_{\text{Jup}}$  exoplanet orbiting the star at 3.6 au. Our study marks the first *direct* detection of HD 206893 c providing highly precise astrometry ( $\sim 50\text{--}100 \mu\text{arcsec}$ ) of the HD 206893 c orbit, as well as medium resolution spectroscopy in the K-band. This discovery establishes HD 206893 as a hybrid planetary system hosting both an exoplanet and a brown dwarf, and therefore presents itself as an exceedingly valuable laboratory for studying possible formation pathways of EGPs and BDs.

## 2. Observations: Precision Radial Velocities and Optical Interferometry

As described in Grandjean et al. (2019a), HD 206893 has been monitored for several years since 2016 with the High Accuracy Radial velocity Planet Searcher (*HARPS*, La Silla, ESO) as part of the Young Nearby Stars survey (YNS; Lagrange et al. 2013). The Spectroscopic data via Analysis of the Fourier Interspectrum RVs (*SAFIR*) software (Galland et al. 2005) was used to compute the RV signal. Figure 1 (*left panel*) shows the processed historical RV datasets taken from Grandjean et al. (2019a) that were used in this study to predict the semi-major axis of HD 206893 c. The residuals between the RV data points and the posterior curves shown in the figure are likely due to stellar pulsations. As shown in Table B.1, there is an additional  $\sigma_{RV} = 40 \text{ m s}^{-1}$  amplitude best-fit stellar jitter term not currently represented in the uncertainties on the individual RV point shown in Figure 1. However, as discussed in §3.1, such residuals in the RV data will not have a significant impact on the final derived physical parameters for HD 206893 c.

All the *GRAVITY* observations presented in this paper were acquired using the dual-field/on-axis mode, with medium spectral resolution ( $R=500$ ). We closely followed the observing strategy outlined in Gravity Collaboration et al. (2019), where the science fiber is alternately centered on the star to obtain the phase reference, and on the position of HD 206893 c. In Appendix A, we provide much more detail regarding the observations obtained using *GRAVITY*.

## 3. Results

### 3.1. Orbit Fits

To assess the orbital parameters for HD 206893 B and c, we employ the method presented in Lacour et al. (2021) to perform Bayesian parameter estimation with the *orbitalize!* (Blunt et al.

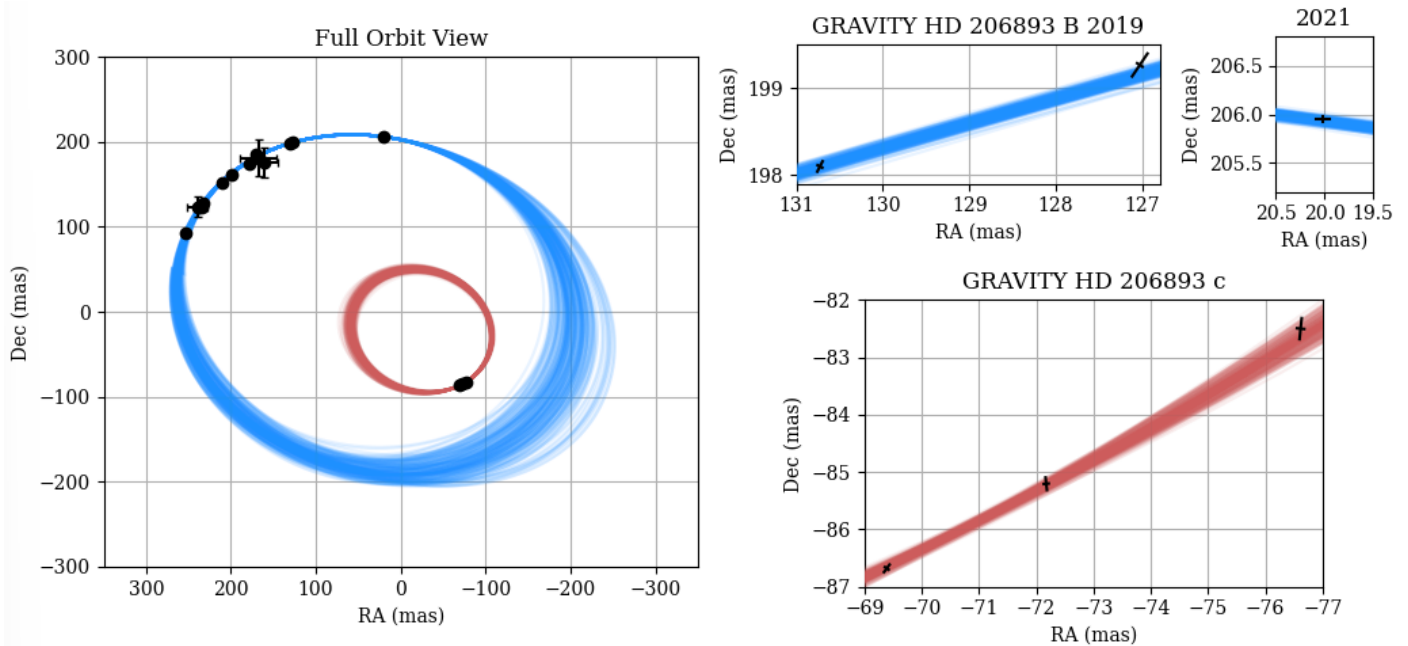


**Fig. 2.** A diagram showing the class of orbits consistent with the measured astrometry for HD 206893 B (blue orbits), and HD 206893 c (red orbits). The HD 206893 B astrometry comes from astrometry obtained in Milli et al. (2017); Delorme et al. (2017); Grandjean et al. (2019a); Stolker et al. (2020); Ward-Duong et al. (2021), as well as the recent GRAVITY detections. The right panels are magnifications (50–100x) of portions of the orbits highlighting the  $\sim 50$  microarcsecond astrometric precision.

2020) software package for jointly fitting the orbits of multiple substellar companions using relative astrometry from GRAVITY, the stellar RVs described in the previous section, and Hipparcos and Gaia absolute stellar astrometry from the EDR3 edition of the HGCA (Brandt 2021; Kervella et al. 2022). This method accounts for shifts in the system barycenter due to multiple planets in the system, but does not account for planet-planet interactions, which are negligible on these timescales. The covariances of the uncertainties in RA/Dec due to  $u$ - $v$  coverage are also automatically handled by `orbitize!`. To find the best fit orbits for the HD 206893 B and c objects, the parallel-tempered affine-invariant sampler (Foreman-Mackey et al. 2013; Vouden et al. 2016) was run using 20 temperatures, 1000 walkers per temperature, and 60,000 steps per walker. The walker chains were visually inspected for convergence, and the last 10,000 steps from each walker at the lowest temperature was used to form the posterior distributions for each parameter. A depiction of the orbits for both HD 206893 B and c are shown in Fig 2.

The results of our MCMC orbital fits are shown in Fig. 2 and summarized in Table 1. The best estimate of the mass and semimajor axis of HD 206893 c is  $12.3^{+1.1}_{-1.2} M_{\text{Jup}}$  and  $3.53^{+0.08}_{-0.07}$  au ( $\sim 5.7$  yr orbital period) for a dynamical fit that incorporates the precise RV monitoring from HARPS. Excluding the RV information from the fit results in values of  $11.6^{+1.7}_{-2.0} M_{\text{Jup}}$  and  $3.65^{+0.10}_{-0.10}$  au. These values are largely consistent with, but also significantly more precise than, the previous estimations of these parameters for the hypothesized HD 206983c companion of  $8$ – $15 M_{\text{Jup}}$  and  $\lesssim 5.6$  au (Grandjean et al. 2019a; Kammerer et al. 2021). At the same time, our fits demonstrate precise, but significantly non-zero, eccentricity of  $0.41^{+0.03}_{-0.03}$  for HD 206893 c ( $0.37^{+0.05}_{-0.05}$  excluding the RV measurements). For completeness we also summarize the results of our orbital fit for HD 206893 B. We find a mass and semi-major axis of  $27.4^{+2.3}_{-2.2} M_{\text{Jup}}$  and  $9.7^{+0.4}_{-0.3}$  au corresponding to a  $\sim 26$  yr orbital period ( $26.5^{+3.0}_{-3.1} M_{\text{Jup}}$  and  $9.7^{+0.6}_{-0.3}$  au excluding the RV measurements). More detail

on the orbit fitting, including the orbital alignment parameters (e.g.,  $i$ ,  $\omega$ ,  $\Omega$ ) can be found in § B of the appendix, as well as Table B.1. As with the case of HD 206893 c, this mass value for HD 206893 B is consistent with, but also significantly more precise than, previous estimates (e.g. Grandjean et al. 2019a; Meshkat et al. 2021; Ward-Duong et al. 2021; Kammerer et al. 2021) that quoted a mass of  $5$ – $30 M_{\text{Jup}}$ , and clearly places HD 206893 B in the low-mass brown dwarf regime.

### 3.2. Models Incorporating Enhanced Helium Abundance

In §3.3, we describe our procedure to fit the GRAVITY spectroscopy with a grid of synthetic atmospheric models. Despite the significantly different dynamical masses derived for HD 206893 B and c, the similarity in bolometric luminosities for both components is striking:  $\log(L/L_{\odot}) \approx -4.23$  versus  $-4.42$  for B and c, respectively. Thus, assuming a coeval formation for the two objects, standard hot-start evolutionary models (e.g., Burrows et al. 1997; Baraffe et al. 2003; Baraffe et al. 2015) cannot simultaneously provide a solution for the brightness of both objects. Adjusting the initial entropy (Spiegel & Burrows 2012; Marleau & Cumming 2014) of either object within these evolutionary models does not ease the tension. Indeed, an elevated initial entropy will not increase the luminosity of c at its present age of  $\approx 200$  Myr because this is already greater than its initial cooling timescale (Marleau & Cumming 2014). Similarly, no reasonable lower initial entropy for B could sufficiently delay the onset of deuterium burning so that it would be observed in the rising part of a “deuterium flash” (see Fig. 8 of Marleau & Cumming 2014 or Fig. 13 of Bonnefoy et al. 2014).

Instead, the puzzle of a single set of models being unable to simultaneously account for the luminosities of both objects can be addressed by letting c burn deuterium significantly. With a classical value of  $(13 \pm 0.8) M_{\text{Jup}}$  for the mass above which an object burns more than 50% of its initial deuterium content

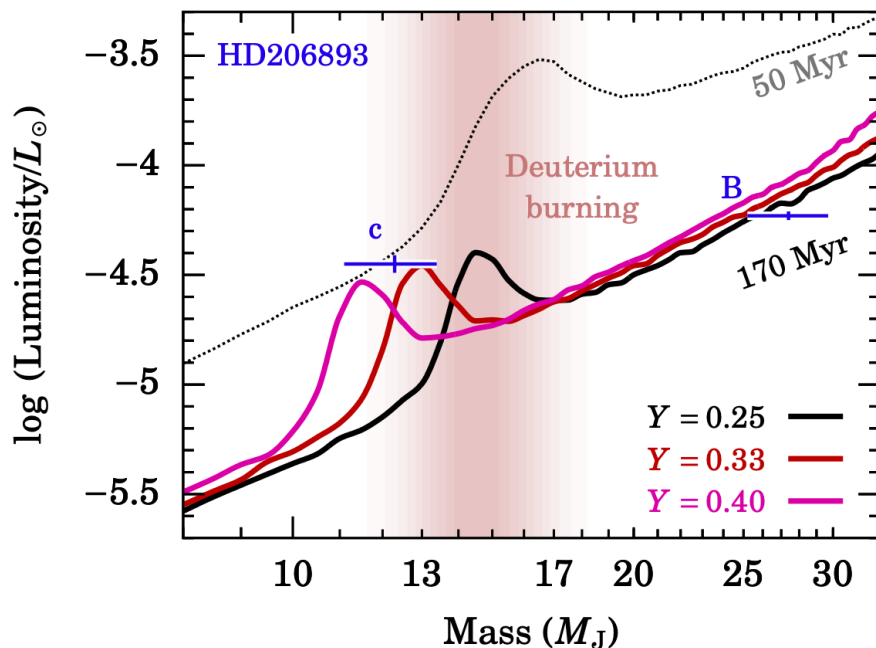


**Fig. 3.** Hot-start isochrones from Marleau & Cumming (2014) but coupled to Baraffe et al. (2003) as in Marleau et al. (2019) with helium fraction ranging from  $Y = 0.25$  to  $0.40$  (solid lines), compared to the dynamical masses and retrieved luminosities of HD 206893 B and c. With the baseline helium content  $Y = 0.25$ , the 170 Myr isochrone (solid black curve) matches the bolometric luminosity of HD 206893 B assuming a mass of  $27 M_{\text{Jup}}$  but does not match c, and conversely for the 50 Myr isochrone (dotted black, with  $Y = 0.25$ ). Increasing the helium abundance to  $Y = 0.33$  could nearly explain the measurements of both components of the HD 206893 system.

(Spiegel et al. 2011), nuclear reactions do not slow down the cooling of c significantly even at an upper-one-sigma mass of  $13.4 M_{\text{Jup}}$ . However, Spiegel et al. (2011) and Mollière & Mordasini (2012) have shown that varying the helium, deuterium, or metal content of an object can shift the D-burning mass boundary significantly, with  $11.8 M_{\text{Jup}}$  a plausible value. If both objects are co-eval, the proximity of c to the deuterium-burning limit makes it possible to let it be in a deuterium-burning phase by varying model parameters while not affecting the modeled luminosity of B. Because of its higher mass, it is already past its deuterium-burning phase, which, for hot starts, occurs earlier at high mass.

The simplest adjustment is to increase the bulk deuterium abundance but quantitatively this is problematic. From our tests (not shown), a model that is consistent with the brightness of HD 206893 c would call for a deuterium number fraction relative to hydrogen several times higher than in the local interstellar medium,  $D/H = (2.0 \pm 0.1) \times 10^{-5}$  (Prodanović et al. 2010), or the  $(2.57 \pm 0.03) \times 10^{-5}$  value from Big Bang Nucleosynthesis (BBN) estimates (Fields et al. 2014). The latter is effectively an absolute upper limit because no process can increase the bulk abundance of deuterium; it can only be destroyed.

A more realistic route is to enhance the helium mass fraction,  $Y$ , to explain the overluminosity of HD 206893 c. An elevated helium fraction can serve as a proxy for an overall heavier composition (Baraffe et al. 2006, 2008), representing an approximately normal helium abundance along with a higher bulk metallicity. Physically, a heavier composition leads to a more compact planet with correspondingly higher internal temperatures, in turn leading to enhanced deuterium burning at lower masses. Also, deriving a heavy element content (helium and metals) abundance from such models could help place constraints on formation locations within the primordial protoplanetary disk (Cridland et al. 2016; Mollière et al. 2022).

Therefore, we use the models of Marleau & Cumming (2014) to model the luminosity of substellar objects as a function of their mass and age. We have extended them to use the Baraffe et al. (2003) atmospheric boundary condition as in the BEX models (Marleau et al. 2019), and have generated grids of models with different  $Y$  values and going up to high masses. Figure 3 shows an example of these model isochrones at an age of 170 Myr for hot starts (here, an initial entropy of  $13.5 k_{\text{B}}$  baryon $^{-1}$ ) and a helium fraction ranging from  $Y=0.25$  to  $0.40$ . For reference, a curve is also shown assuming a younger age of 50 Myr, consistent with the luminosity of the c companion but not B. It is notable that the curve assuming a 170 Myr age and a baseline abundance of  $Y = 0.25$  cannot simultaneously account for the luminosities of HD 206893 B and c (at the level of  $\sim 2\sigma$  in the mass coordinate). However, by varying the level of helium enrichment, solutions can be found assuming an age of 170 Myr for both. This is because the luminosities of lower-mass objects ( $\sim 12\text{--}17 M_{\text{Jup}}$ ) near the deuterium burning limit can vary at a fixed age of 170 Myr by a factor of a few up to an order of magnitude depending on the helium fraction. Thus, using these models, we find that a 170 Myr model assuming a helium fraction of  $Y = 0.33$  could account for the luminosities of both components of the HD 206893 system. For this exploratory analysis we match the data only at approximately  $1\sigma$  of both mass values, and will attempt a more careful fit in a future work.

As a check, we have run similar models using the MESA stellar evolution code (Paxton et al. 2011, 2019). The results are largely in line with the discussion above. Indeed, adjusting these parameters within MESA (e.g., D/H, helium abundance, etc.) one by one, we can reproduce the luminosity for HD 206893 c to within a factor of  $\sim 2$ . These tests give confidence that our results are not representing any approximations inherent in the Marleau & Cumming (2014) models.

Quantity	Dynamical fit	Model Grid Fit
<b>HD 206893 c</b>		
$M_c [M_{\text{Jup}}]$	$12.3_{-1.2}^{+1.1}$ ( $11.6_{-2.0}^{+1.7}$ )	—
$a_c$ [au]	$3.53_{-0.07}^{+0.08}$ ( $3.65_{-0.10}^{+0.10}$ )	—
$e_c$ au	$0.41_{-0.03}^{+0.03}$ ( $0.37_{-0.05}^{+0.05}$ )	—
$R_c$ [ $R_{\text{Jup}}$ ]	—	$1.46_{-0.06}^{+0.18}$
$T_{\text{eff}}$ [K]	—	$1181.9_{-53.9}^{+20.6}$
$\log g$	—	$4.08_{-0.18}^{+0.10}$
$\log(L/L_{\odot})$	—	$-4.42_{-0.01}^{+0.02}$
<b>HD 206893 B</b>		
$M_B [M_{\text{Jup}}]$	$27.4_{-2.2}^{+2.3}$ ( $26.5_{-3.1}^{+3.0}$ )	—
$a_B$ au	$9.7_{-0.3}^{+0.4}$ ( $9.7_{-0.3}^{+0.6}$ )	—
$e_B$ au	$0.14_{-0.05}^{+0.05}$ ( $0.12_{-0.07}^{+0.06}$ )	—
$R_B$ [ $R_{\text{Jup}}$ ]	—	$1.25_{-0.02}^{+0.02}$
$T_{\text{eff}}$ [K]	—	$1429.2_{-6.2}^{+5.6}$
$\log g$	—	$4.66_{-0.04}^{+0.04}$
$\log(L/L_{\odot})$	—	$-4.23_{-0.01}^{+0.01}$

**Table 1.** Orbital and physical parameters for HD 206893 c, and re-evaluated parameters of HD 206893 B. Values not listed in parentheses are those which utilise both the astrometry and RVs during the dynamical orbit fit, while those contained in parenthesis exclude the RV measurements. The model fit refers to a fit of a grid of DRIFT-PHOENIX models assuming no additional dust, and using mass priors of  $26 \pm 2$  and  $12 \pm 1 M_{\text{Jup}}$  for B and c, respectively.

Importantly, since the luminosity of HD 206893 B is not strongly affected by the initial deuterium or the helium abundance in the models, this object can be considered as an independent “chronometer” of the system. Assuming the two members of the system to be coeval<sup>1</sup>, this lets our models set constraints on the bulk properties of HD 206893 c. The pink shaded region in Fig. 3 highlights approximately the mass range in which deuterium burning keeps the luminosity significantly higher at a given age than for neighbouring masses. It is a clear prediction of these models that after several hundred million years the deuterium burning will cease, leaving HD 206893 c (again, in this plot at the upper  $1\sigma$  limit of the mass) squarely in the luminosity regime typically associated with planets rather than brown dwarfs.

It is not clear what process(es) could increase the bulk concentration of helium to  $Y = 0.33$ , but our result should be taken more broadly to indicate that non-standard parameter values for the cooling curves are required to reproduce the observations. In a forthcoming paper, this will be given a detailed statistical treatment by varying systematically the initial entropies of the objects, their core masses, deuterium abundances, and so on. In any case, the distance in Fig. 3 between the data points and the standard models is too large to be explained by simple measurement errors or small model uncertainties.

<sup>1</sup> Even for an age of 50 Myr, the formation time of at most several million years is a negligibly short fraction of the system’s age.

### 3.3. GRAVITY Spectroscopy of HD 206893 c: Model Grid Fits to Derive Atmospheric Parameters

To estimate the primary atmospheric parameters of HD 206893 c (e.g., effective temperature, radius, and bolometric luminosity) we utilize the methodology outlined in Kammerer et al. (2021) to fit the GRAVITY spectroscopy shown in Fig. 4 with a grid of DRIFT-PHOENIX models (Helling et al. 2008) using the species toolkit described in Stolker et al. (2020). Selecting these models to fit the spectroscopy of HD 206893 c has the advantage that the model fits are consistent with those carried out in Kammerer et al. (2021) for the HD 206893 B companion in the sense that the same underlying assumptions were made for the dust properties and atmospheric physics. Moreover, among the three different model grids used in Kammerer et al. (2021), the DRIFT-PHOENIX grid is the only one that yields a good fit to the extremely red colors of HD 206893 B without including an additional source of reddening. Even if the DRIFT-PHOENIX grid does not fully capture the full physical picture of the atmosphere, the models empirically fit well, and thus are effective for measuring the bolometric luminosity.

The best fit parameters for HD 206893 B and c are shown in Table 1, and the best fit DRIFT-PHOENIX spectra together with our GRAVITY spectra of both companions as well as other spectrophotometry of B from the literature are shown in Fig. 4. It should be noted that the derived bolometric luminosity,  $L_{\text{bol}}$ , is indeed dependent on the chosen atmospheric model, so there may be additional systematic uncertainties due to these differences between models. However, the derived effective temperature ( $T_{\text{eff}}$ ) and radius ( $R$ ) are typically negatively correlated, which reduces the variation in the derived  $L_{\text{bol}}$  across multiple models. To verify this, for multiple atmospheric models we have compared the  $L_{\text{bol}}$  calculated from  $T_{\text{eff}}$  and  $R$  to that calculated by integrating the full model spectrum, and the agreement is typically a ~few percent, consistent with the uncertainties in  $L_{\text{bol}}$  presented here.

## 4. Discussion

Despite the promise shown by the isochronal models incorporating a higher overall helium abundance potentially leading to the onset of deuterium burning, some caution should be exercised by such a simple parameterization. This study should be thought of as more of an initial exploratory, heuristic analysis. Indeed, it may be that the enhanced helium abundance is acting as a proxy for (possibly a combination of) other internal physics within this system. For example, varying the core mass, or similarly the abundance or distribution of heavy elements, or choosing different atmospheric models will have the effect of altering the isochrones and the quantitative constraint on the helium or initial deuterium fractions. Nonetheless, it is unlikely that adjusting the atmospheric parameters within a model for HD 206893 c could lead to a bolometric luminosity that is enhanced by nearly an order of magnitude relative to model predictions.

Systematic errors in our dynamical analysis leading to an erroneous calculated value of the mass of HD 206893 c are also most likely a remote possibility. Our calculation of the dynamical mass uses a combination of stellar astrometry that may have systematic uncertainties that are not well understood, as well as RV measurements that are impacted by stellar activity (e.g., Grandjean et al. 2019a). However, Table 1 shows that excluding the RV data from our fits gives very similar calculated values for the mass of HD 206893 c ( $12.3_{-1.2}^{+1.1} M_{\text{Jup}}$  versus  $11.6_{-2.0}^{+1.7} M_{\text{Jup}}$  with the RVs excluded). It should be noted that in this analy-

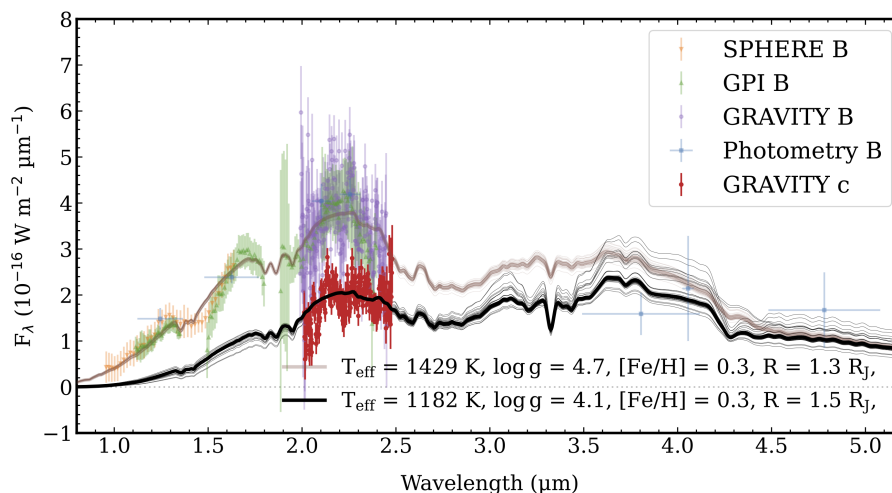


**Fig. 4.** Combined  $R \sim 500$  GRAVITY K-band spectra of HD 206893 c and B (red and light purple, respectively) together with the best fit DRIFT-PHOENIX models (black and light brown). Shown in light orange, green, and blue is archival spectrophotometry of B that was also included in the fit. For the model spectra, several samples drawn from the posterior distribution are shown with thin lines.

sis we did not model the stellar activity in our orbit fit, which may contribute to a slight bias. However, it is unlikely that such unknown systematic errors within our analysis have significantly biased our calculated masses, especially given that our measured dynamical mass of HD 206893 c is very much consistent with the predictions presented in Grandjean et al. (2019a) and Kammerer et al. (2021). At most, these systematics could have led to underestimated astrometric uncertainties, but this would not have changed the overall conclusions of this study.

## 5. Conclusions

We have presented the discovery of an inner  $\sim 12 M_{\text{Jup}}$  exoplanet at 3.5 au in the HD 206893 system, making this one of the first directly imaged “hybrid” planetary systems containing both a brown dwarf (Milli et al. 2017) and a bona fide exoplanet. This is also an example of a discovery of an additional companion following a previous discovery of an outer one (e.g., Lagrange et al. 2019; Nowak et al. 2020). The highly precise astrometry delivered by GRAVITY ( $\sim 50\text{--}100 \mu\text{arcsec}$ ) has enabled us to derive precise dynamical masses of  $12.3^{+1.1}_{-1.2} M_{\text{Jup}}$  for HD 206893 c and  $27.4^{+2.3}_{-2.2} M_{\text{Jup}}$  for HD 206893 B. The dynamical mass of B, combined with its luminosity, allows us to immediately and unambiguously establish a robust age of  $\sim 200$  Myr for this system. Using the mass/luminosity for c, our modified isochronal model allows us to fine tune this value to  $\sim 170$  Myr. This is the first time to our knowledge that the *age* of a system has been constrained using the dynamically measured masses of orbiting companions. Further, having both an EGP and a BD in the same system, with a common age, HD 206893 will serve as an extraordinarily valuable system for the purpose of furthering our understanding of planet formation, and highlighting distinctions between the formation pathways of EGPs and BDs. The analysis of the dynamical stability presented in Appendix D demonstrates that this system is much closer to instability than e.g., the  $\beta$  Pictoris system.

By establishing a precise age for the system, we have used modified models taken from Marleau & Cumming (2014) to show that one possible solution to the anomalously similar luminosities of HD 206893 B and c is an increased helium abundance in the system. An elevated helium abundance will result in elevated deuterium burning, and *could* account for the anomalously

high luminosity of the c component. However, the key takeaway from this study is that non-standard cooling curves are required to provide a good match to the data. Besides residing in a hybrid exoplanetary system, HD 206893 c is an object straddling the deuterium-burning limit, and thus is an ideal laboratory to establish the precise mass where this process can occur. In addition to having a dramatic impact on its evolution, the duration and extent of deuterium burning in a substellar object may give valuable clues to its initial conditions and internal structure (e.g., the presence/lack of a rocky core, initial entropy, and initial deuterium abundance, Spiegel & Burrows 2012; Mollière & Mordasini 2012; Bodenheimer et al. 2013; Mordasini 2013). Ours is the first such study to begin addressing these questions, and additional studies like this may help to craft a more robust discrimination between EGPs and BDs.

Finally, in addition to being only the second directly imaged exoplanet whose presence was hinted at using the RV method, our precise dynamical mass for HD 206893 c means that this effort potentially represents the first discovery via direct imaging of a bona fide exoplanet that partially relies on precise measurements of the host star astrometry from the *Gaia* mission. This complements numerous other recent discoveries of substellar companions (e.g., Bonavita et al. 2022; Kuzuhara et al. 2022; Franson et al. 2022, Currie et al. *in preparation*) whose discovery also utilized *Gaia* astrometry. Using precise host star *Gaia* astrometry to point the way to orbiting planets suitable for direct imaging is expected to be one of the primary strategies for direct exoplanet detection and characterization going forward, thereby ending the current era of direct imaging EGP searches that have had notoriously low detection rates (e.g., Bowler & Nielsen 2018). Secondly, recent exoplanet direct imaging surveys have had limited sensitivity (e.g. Nielsen et al. 2019; Vigan et al. 2021) to the peak of the orbital distribution of giant exoplanets that coincides with the location of the water ice line at 2-3 au for solar type stars (e.g., Fernandes et al. 2019; Freikh et al. 2019; Fulton et al. 2021). Along with the discovery of  $\beta$  Pic c (Lagrange et al. 2019; Nowak et al. 2020) this discovery of an exoplanet at 3.5 au is more evidence that optical interferometry now enables direct characterization of these planets at the ice-line orbital separations of 2-3 au *where they form*.

**Acknowledgements.** G-DM acknowledges the support of the DFG priority program SPP 1992 “Exploring the Diversity of Extrasolar Planets” (MA 9185/1) and from the Swiss National Science Foundation under grant 200021\_204847 “PlanetsInTime”. Parts of this work have been carried out within the framework of the NCCR PlanetS supported by the Swiss National Science Foundation. P.M. acknowledges support from the European Research Council under the European Union’s Horizon 2020 research and innovation program under grant agreement No. 832428-Origins. This research has made use of the SIMBAD database, operated at CDS, Strasbourg, France. This work has made use of data from the European Space Agency (ESA) mission *Gaia* (<https://www.cosmos.esa.int/gaia>), processed by the *Gaia* Data Processing and Analysis Consortium (DPAC, <https://www.cosmos.esa.int/web/gaia/dpac/consortium>). Funding for the DPAC has been provided by national institutions, in particular the institutions participating in the *Gaia* Multilateral Agreement.

## References

- Baraffe, I., Alibert, Y., Chabrier, G., & Benz, W. 2006, *A&A*, 450, 1221
- Baraffe, I., Chabrier, G., & Barman, T. 2008, *A&A*, 482, 315
- Baraffe, I., Chabrier, G., Barman, T. S., Allard, F., & Hauschildt, P. H. 2003, *Astronomy and Astrophysics*, 402, 701
- Baraffe, I., Homeier, D., Allard, F., & Chabrier, G. 2015, *A&A*, 577, A42
- Beust, H., Bonfils, X., Montagnier, G., Delfosse, X., & Forveille, T. 2012, *A&A*, 545, A88
- Blunt, S., Wang, J. J., Angelo, I., et al. 2020, *Astronomical Journal*, 159, 89
- Bodenheimer, P., D’Angelo, G., Lissauer, J. J., Fortney, J. J., & Saumon, D. 2013, *ApJ*, 770, 120
- Bonavita, M., Fontanive, C., Gratton, R., et al. 2022, *MNRAS*, 513, 5588
- Bonnefoy, M., Currie, T., Marleau, G. D., et al. 2014, *A&A*, 562, A111
- Bowler, B. P., Liu, M. C., Shkolnik, E. L., & Dupuy, T. J. 2013, *ApJ*, 774, 55
- Bowler, B. P. & Nielsen, E. L. 2018, Occurrence Rates from Direct Imaging Surveys, *Handbook of Exoplanets* (Springer International Publishing AG), 155
- Brandt, T. D. 2021, *Astrophysical Journal Supplement*, 254, 42
- Burrows, A., Marley, M., Hubbard, W. B., et al. 1997, *ApJ*, 491, 856
- Chabrier, G., Baraffe, I., Selsis, F., et al. 2007, *Protostars and Planets V*, 623
- Chen, C. H., Mittal, T., Kuchner, M., et al. 2014, *Astrophysical Journal Supplement*, 211, 25
- Cridland, A. J., Pudritz, R. E., & Alessi, M. 2016, *MNRAS*, 461, 3274
- David, T. J. & Hillenbrand, L. A. 2015, *Astrophysical Journal*, 804, 146
- Delorme, P., Schmidt, T., Bonnefoy, M., et al. 2017, *Astronomy & Astrophysics*, 608, A79
- Fabrycky, D. & Tremaine, S. 2007, *ApJ*, 669, 1298
- Fernandes, R. B., Mulders, G. D., Pascucci, I., Mordasini, C., & Emsenhuber, A. 2019, *ApJ*, 874, 81
- Fields, B. D., Molaro, P., & Sarkar, S. 2014, arXiv e-prints, arXiv:1412.1408
- Foreman-Mackey, D., Hogg, D. W., Lang, D., & Goodman, J. 2013, *Publications of the Astronomical Society of the Pacific*, 125, 306
- Franson, K., Bowler, B. P., Brandt, T. D., et al. 2022, *AJ*, 163, 50
- Freikh, R., Jang, H., Murray-Clay, R. A., & Petrovich, C. 2019, *ApJ*, 884, L47
- Fulton, B. J., Rosenthal, L. J., Hirsch, L. A., et al. 2021, *ApJS*, 255, 14
- Gaia Collaboration, Brown, A. G. A., Vallenari, A., et al. 2018, *Astronomy & Astrophysics*, 616, A1
- Gaia Collaboration, Brown, A. G. A., Vallenari, A., et al. 2021, *A&A*, 649, A1
- Gaia Collaboration, Prusti, T., de Bruijne, J. H. J., et al. 2016, *A&A*, 595, A1
- Galland, F., Lagrange, A. M., Udry, S., et al. 2005, *Astronomy & Astrophysics*, 443, 337
- Gáspár, A., Rieke, G. H., & Ballering, N. 2016, *ApJ*, 826, 171
- Grandjean, A., Lagrange, A. M., Beust, H., et al. 2019a, *Astronomy & Astrophysics*, 627, L9
- Grandjean, A., Lagrange, A. M., Beust, H., et al. 2019b, *A&A*, 629, C1
- Gravity Collaboration, Abuter, R., Accardo, M., et al. 2017, *Astronomy and Astrophysics*, 602, A94
- GRAVITY Collaboration, Abuter, R., Amorim, A., et al. 2021, *A&A*, 647, A59
- Gravity Collaboration, Lacour, S., Nowak, M., et al. 2019, *Astronomy & Astrophysics*, 623, L11
- Gravity Collaboration, Nowak, M., Lacour, S., et al. 2020, *Astronomy and Astrophysics*, 633, A110
- Helling, C., Dehn, M., Woitke, P., & Hauschildt, P. H. 2008, *ApJ*, 675, L105
- Hinkley, S., Pueyo, L., Faherty, J. K., et al. 2013, *ApJ*, 779, 153
- Holmberg, J., Nordström, B., & Andersen, J. 2007, *A&A*, 475, 519
- Kammerer, J., Lacour, S., Stolker, T., et al. 2021, *Astronomy & Astrophysics*, 652, A57
- Kennedy, G. M. & Wyatt, M. C. 2014, *MNRAS*, 444, 3164
- Kervella, P., Arenou, F., & Thévenin, F. 2022, *A&A*, 657, A7
- Kozai, Y. 1962, *AJ*, 67, 591
- Kuzuhara, M., Currie, T., Takarada, T., et al. 2022, arXiv e-prints, arXiv:2205.02729
- Lacour, S., Dembet, R., Abuter, R., et al. 2019, *A&A*, 624, A99
- Lacour, S., Eisenhauer, F., Gillessen, S., et al. 2014, *Astronomy and Astrophysics*, 567, A75
- Lacour, S., Wang, J. J., Nowak, M., et al. 2020, in *Society of Photo-Optical Instrumentation Engineers (SPIE) Conference Series*, Vol. 11446, Society of Photo-Optical Instrumentation Engineers (SPIE) Conference Series, 114460O
- Lacour, S., Wang, J. J., Rodet, L., et al. 2021, *Astronomy & Astrophysics*, 654, L2
- Lagrange, A. M., Meunier, N., Chauvin, G., et al. 2013, *Astronomy & Astrophysics*, 559, A83
- Lagrange, A. M., Meunier, N., Rubini, P., et al. 2019, *Nature Astronomy*, 3, 1135
- Lapeyrere, V., Kervella, P., Lacour, S., et al. 2014, in *Society of Photo-Optical Instrumentation Engineers (SPIE) Conference Series*, Vol. 9146, *Optical and Infrared Interferometry IV*, ed. J. K. Rajagopal, M. J. Creech-Eakman, & F. Malbet, 91462D
- Lazzoni, C., Desidera, S., Marzari, F., et al. 2018, *A&A*, 611, A43
- Madhusudhan, N., Amin, M. A., & Kennedy, G. M. 2014, *ApJ*, 794, L12
- Marino, S., Zurlo, A., Faramaz, V., et al. 2020, *MNRAS*, 498, 1319
- Marleau, G.-D., Coleman, G. A. L., Leleu, A., & Mordasini, C. 2019, *Astronomy and Astrophysics*, 624, A20
- Marleau, G.-D. & Cumming, A. 2014, *MNRAS*, 437, 1378
- Meshkat, T., Gao, P., Lee, E. J., et al. 2021, *Astrophysical Journal*, 917, 62
- Milli, J., Hibon, P., Christiaens, V., et al. 2017, *Astronomy & Astrophysics*, 597, L2
- Mollière, P., Molyarova, T., Bitsch, B., et al. 2022, arXiv e-prints, arXiv:2204.13714
- Mollière, P. & Mordasini, C. 2012, *A&A*, 547, A105
- Moór, A., Ábrahám, P., Derekas, A., et al. 2006, *Astrophysical Journal*, 644, 525
- Mordasini, C. 2013, *A&A*, 558, A113
- Mordasini, C., van Boekel, R., Mollière, P., Henning, T., & Benneke, B. 2016, *ApJ*, 832, 41
- Nederlander, A., Hughes, A. M., Fehr, A. J., et al. 2021, *Astrophysical Journal*, 917, 5
- Netopil, M. 2017, *MNRAS*, 469, 3042
- Nielsen, E. L., De Rosa, R. J., Macintosh, B., et al. 2019, *The Astronomical Journal*, 158, 13
- Nowak, M., Lacour, S., Lagrange, A. M., et al. 2020, *A&A*, 642, L2
- Öberg, K. I., Murray-Clay, R., & Bergin, E. A. 2011, *ApJ*, 743, L16
- Paxton, B., Bildsten, L., Dotter, A., et al. 2011, *ApJS*, 192, 3
- Paxton, B., Smolec, R., Schwab, J., et al. 2019, *ApJS*, 243, 10
- Prodanović, T., Steigman, G., & Fields, B. D. 2010, *MNRAS*, 406, 1108
- Rein, H., Hernandez, D. M., Tamayo, D., et al. 2019, *Monthly Notices of the Royal Astronomical Society*, 485, 5490
- Rein, H. & Liu, S.-F. 2012, *Astronomy & Astrophysics*, Volume 537, id.A128, 10 pp., 537, A128
- Silverstone, M. D. 2000, PhD thesis, University of California, Los Angeles
- Spiegel, D. S. & Burrows, A. 2012, *ApJ*, 745, 174
- Spiegel, D. S., Burrows, A., & Milsom, J. A. 2011, *ApJ*, 727, 57
- Stolker, T., Quanz, S. P., Todorov, K. O., et al. 2020, *Astronomy & Astrophysics*, 635, A182
- Vigan, A., Fontanive, C., Meyer, M., et al. 2021, *A&A*, 651, A72
- Vousden, W. D., Farr, W. M., & Mandel, I. 2016, *Monthly Notices of the Royal Astronomical Society*, 455, 1919
- Ward-Duong, K., Patience, J., Follette, K., et al. 2021, *Astronomical Journal*, 161, 5
- Yelverton, B., Kennedy, G. M., Su, K. Y. L., & Wyatt, M. C. 2019, *MNRAS*, 488, 3588
- Zuckerman, B. & Song, I. 2004, *Astrophysical Journal*, 603, 738

- 
- <sup>1</sup> University of Exeter, Physics Building, Stocker Road, Exeter EX4 4QL, United Kingdom
  - <sup>2</sup> LESIA, Observatoire de Paris, PSL, CNRS, Sorbonne Université, Université de Paris, 5 place Janssen, 92195 Meudon, France
  - <sup>3</sup> European Southern Observatory, Karl-Schwarzschild-Straße 2, 85748 Garching, Germany
  - <sup>4</sup> Fakultät für Physik, Universität Duisburg-Essen, Lotharstraße 1, 47057 Duisburg, Germany
  - <sup>5</sup> Institut für Astronomie und Astrophysik, Universität Tübingen, Auf der Morgenstelle 10, 72076 Tübingen, Germany
  - <sup>6</sup> Center for Space and Habitability, Universität Bern, Gesellschaftsstrasse 6, 3012 Bern, Switzerland
  - <sup>7</sup> Max Planck Institute for Astronomy, Königstuhl 17, 69117 Heidelberg, Germany
  - <sup>8</sup> Université Grenoble Alpes, CNRS, IPAG, 38000 Grenoble, France
  - <sup>9</sup> Department of Astronomy, California Institute of Technology, Pasadena, CA 91125, USA
  - <sup>10</sup> Space Telescope Science Institute, Baltimore, MD 21218, USA
  - <sup>11</sup> Institute of Astronomy, University of Cambridge, Madingley Road, Cambridge CB3 0HA, United Kingdom
  - <sup>12</sup> Center for Astrophysics and Planetary Science, Department of Astronomy, Cornell University, Ithaca, NY 14853, USA
  - <sup>13</sup> Department of Physics & Astronomy, Johns Hopkins University, 3400 N. Charles Street, Baltimore, MD 21218, USA
  - <sup>14</sup> Leiden Observatory, Leiden University, P.O. Box 9513, 2300 RA Leiden, The Netherlands
  - <sup>15</sup> Department of Physics, University of Warwick, Coventry CV4 7AL, UK
  - <sup>16</sup> Universidade de Lisboa - Faculdade de Ciências, Campo Grande, 1749-016 Lisboa, Portugal
  - <sup>17</sup> CENTRA - Centro de Astrofísica e Gravitação, IST, Universidade de Lisboa, 1049-001 Lisboa, Portugal
  - <sup>18</sup> Max Planck Institute for extraterrestrial Physics, Giessenbachstraße 1, 85748 Garching, Germany
  - <sup>19</sup> Aix Marseille Univ, CNRS, CNES, LAM, Marseille, France
  - <sup>20</sup> School of Physics and Astronomy, Monash University, Clayton, VIC 3800, Melbourne, Australia
  - <sup>21</sup> 1. Institute of Physics, University of Cologne, Zùlpicher Straße 77, 50937 Cologne, Germany
  - <sup>22</sup> Max Planck Institute for Radio Astronomy, Auf dem Hùgel 69, 53121 Bonn, Germany
  - <sup>23</sup> Universidade do Porto, Faculdade de Engenharia, Rua Dr. Roberto Frias, 4200-465 Porto, Portugal
  - <sup>24</sup> School of Physics, University College Dublin, Belfield, Dublin 4, Ireland
  - <sup>25</sup> Astronomy Department, University of Michigan, Ann Arbor, MI 48109 USA
  - <sup>26</sup> European Southern Observatory, Casilla 19001, Santiago 19, Chile
  - <sup>27</sup> European Space Agency (ESA), ESA Office, Space Telescope Science Institute, 3700 San Martin Drive, Baltimore, MD 21218, USA
  - <sup>28</sup> Department of Earth & Planetary Sciences, Johns Hopkins University, Baltimore, MD, USA
  - <sup>29</sup> Department of Astronomy, Smith College, Northampton MA 01063 USA
  - <sup>30</sup> Pixyl S.A. La Tronche, France
  - <sup>31</sup> Department of Physics, University of Oxford, UK
  - <sup>32</sup> Department of Physics and McGill Space Institute, McGill University, 3600 rue University, Montreal QC H3A 2T8, Canada
  - <sup>33</sup> Institut de Recherche sur les Exoplanètes (iREx), Université de Montréal, C.P. 6128 Succ. Centre-ville, Montreal, QC H3C 3J7, Canada
  - <sup>34</sup> Academia Sinica, Institute of Astronomy and Astrophysics, 11F Astronomy-Mathematics Building, NTU/AS campus, No. 1, Section 4, Roosevelt Rd., Taipei 10617, Taiwan
  - <sup>35</sup> Advanced Concepts Team, European Space Agency, TEC-SF, ESTEC, Keplerlaan 1, 2201 AZ Noordwijk, The Netherlands

## Appendix A: GRAVITY Observations

These observations were reduced using the procedure described in Gravity Collaboration et al. (2020) and Nowak et al. (2020). The coherent flux is extracted for the on-star and on-planet exposures using the GRAVITY pipeline (Lapeyrere et al. 2014). The on-planet data are then phase-referenced to the on-star observations, and the data are fitted with a model which includes both a planet component and a low-order polynomial (for speckle deconvolution). The astrometry is obtained by varying the astrometry of the planet component, and looking for the minimum  $\chi^2$ , or, equivalently, by maximising the periodogram power. More details are provided in Appendix A.1 as well as Appendix B in Nowak et al. (2020)).

Following the work from Kammerer et al. (2021), we used the previous GRAVITY astrometry of HD 206893 B in combination with the new HARPS observations (Grandjean et al. 2019a,b) and DR3 astrometry (Gaia Collaboration et al. 2016, 2021) to predict a position for HD 206893 c in August 2021. The previous GRAVITY astrometry measurements were particularly useful for constraining the orbit of HD 206893 B, and subsequently remove its signal from the RV data and *Gaia* astrometry. The RV data were particularly useful for constraining the period, and thus the semi-major axis of HD 206893 c, while the *Gaia* astrometry provided constraints on its position angle. During the two nights between the 26<sup>th</sup> and 28<sup>th</sup>, we used the GRAVITY instrument (Gravity Collaboration et al. 2017) to try to detect the exoplanet. GRAVITY only probes a small circular region of  $\sim 50$  mas radius around the position of the single mode fiber. We searched for the companion over a region of the order of  $10\,000\text{ mas}^2$  by offsetting the science fiber of the instrument. At the same time the fringe tracker observed the star to correct atmospheric turbulence (Lacour et al. 2019). This allowed an integration time of several tens of seconds. The log of the observations, as well as the position of the single mode fibers, are summarised in Table A.1. During the second night, on the last pointing, a weak signal was detected. The exoplanet position was confirmed one month later, in September. Detection was obtained during runs ID 1104.C-0651, part of the ExoGRAVITY large program (Lacour et al. 2020), and the confirmation during a dedicated run (ID 105.20T0.001). In October, a final observation was carried out, as part of the ExoGRAVITY large program, with the goal of obtaining a good calibration of the spectrum. Section A.1 below gives examples of the periodogram power maps obtained from our observations, both for a non-detection (fiber mispointed during the search), and for a detection of the planet. The *K*-band contrast relative to the host star for HD 206893 c is approximately  $8.2 \times 10^{-5}$ , compared to  $1.6 \times 10^{-4}$  for HD 206893 B.

The astrometry obtained at the three epochs are given in Table A.2. In addition to HD 206893 c, we have recomputed the astrometry of the HD 206893 B from the Kammerer et al. (2021) paper, and added an extra position obtained in August 2021. With respect to the theoretical performance of GRAVITY ( $10\ \mu\text{as}$ , Lacour et al. 2014), the astrometry accuracy is still a factor 5 to 20 worse. The difference during the night of the 27<sup>th</sup> of August can be explained by the mispointing of the science fiber while searching for the exoplanet. The error bars still do not decrease considerably during the other runs because of the limitation due to systematics, particularly the optical aberrations within the fiber injection optics (GRAVITY Collaboration et al. 2021).

### Appendix A.1: Significance of the Detection

In Fig. A.1 we show an example of the periodogram power maps for three observations of HD 206893 c: one in August 2021, obtained when the fiber was mispointed during the search, and two obtained in September and October 2021, when the fiber was properly centered on the planet. Each of the three maps represents the field of view of the GRAVITY science fiber. A clear peak with some sidelobes in periodogram power (not visible in the August 2021 observation) are characteristic of a successful detection, and give the position of the planet.

## Appendix B: Detailed Orbit Fitting Results

We use the default orbital basis in Blunt et al. (2020). The only difference is that  $\tau$ , the epoch of periastron after a given reference epoch in units of orbital period, uses a reference epoch of MJD 59000. To fit the radial velocity data, we also include two free parameters to fit for a bulk offset in the radial velocity ( $\gamma_{RV}$ ) and a jitter term to inflate the error bars on the radial velocity data to better account for stellar activity ( $\sigma_{RV}$ ). We list the median and 68-percentile credible intervals centered about the median as the error bars in Table B.1. We also computed orbital periods ( $P_B$  and  $P_C$ ) for both companions as well as the mutual inclination of their orbits and listed those in Table B.1.

## Appendix C: HD 206893 Debris Structure

HD 206893 also hosts a prominent debris disk indicated by a high fractional luminosity of  $L_{\text{dust}}/L_{\star} = 2.3 \times 10^{-4}$  (Moór et al. 2006). The disk was originally identified by the *ISO* instrument (Silverstone 2000), and subsequently characterised in greater detail with *Spitzer* (Chen et al. 2014), *Herschel* and *ALMA* observations (Milli et al. 2017; Marino et al. 2020; Nederlander et al. 2021). Marino et al. (2020) imaged the disk with *ALMA*, finding that the radial structure is broad, extending from 30 to 180 au, with a 27 au wide gap at 74 au. We have re-analyzed the *Spitzer* IRS spectrum of HD 206893 c to recalculate the temperature of the 499 K warm dust component found by Chen et al. (2014) to be consistent with the methods described in Kennedy & Wyatt (2014). Our reconstruction of the star + disk spectrum using the methods described by Yelverton et al. (2019) is consistent with a single dust component with a temperature of approximately 50 K. The inner disk edge is therefore likely consistent with inner truncation through interaction with HD 206893 B. Following the method presented in Lazzoni, C. et al. (2018), we analytically estimated that the region cleared from dust due to the presence of the two planets extends from  $\sim 1.5$  au to  $\sim 15.5$  au. Since the clearing zone of the planets cannot cover the outer extent of the gap, detected at 30 au (Marino et al. 2020), this could imply the presence of a third smaller planet responsible for shaping the inner edge of the disk

## Appendix D: Dynamical Analysis

Various dynamical considerations can be made from the results of the orbital fit. First, we note that the orbital architecture of the companions does not exhibit a clear resonant configuration. Indeed, as can be seen in Fig. D.1, the probability distribution of the period ratio lies between the 4 : 1 and 5 : 1, and favours instead 9 : 2, which corresponds to a 7<sup>th</sup> order mean-motion resonance (MMR). Such a high-order MMR is not strong enough to induce the libration of a resonant angle, especially when the companions are so massive. Thus, we do not expect resonant

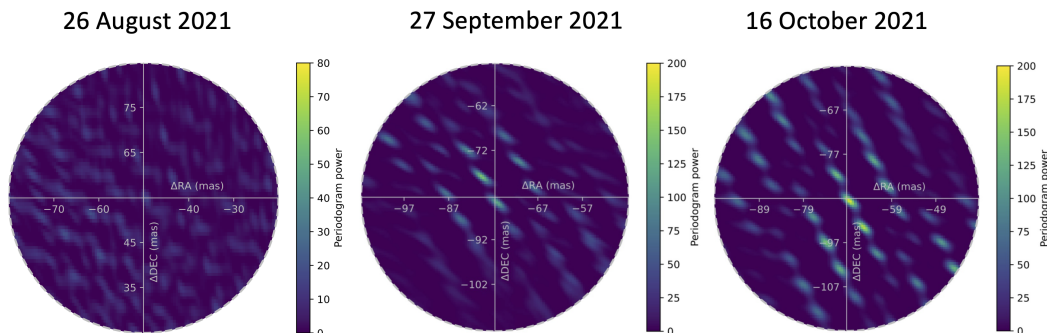


**Fig. A.1.** Periodogram power maps, similar to the one presented in Nowak et al. (2020), obtained for three different observations of HD 206893 c: one resulting in a non-detection during the search for the planet (in August 2021), and two clear detections in September and October 2021.

Date	UT time Start/End	Airmass	$\tau_0$ [ms]	Seeing [ $''$ ]	NEXP/NDIT/DIT	$\Delta$ RA/ $\Delta$ DEC [mas]
2021-08-27	01:14:57 / 03:41:51	1.03–1.35	3.6–7.0	0.5–0.9		
<b>Target:</b>	HD 206893 A				6/64/1 s	0/0
<b>Target:</b>	HD 206893 B				4/16/30 s	17/201
<b>Target:</b>	HD 206893 (no det)				4/32/10 s	-20/72
<b>Target:</b>	HD 206893 (no det)				4/32/10 s	-50/54
<b>Target:</b>	HD 206893 (no det)				4/32/10 s	-70/30
2021-08-28	01:55:39 / 03:55:29	1.02–1.18	4.8–7.4	0.6–0.9		
<b>Target:</b>	HD 206893 A				6/64/1 s	0/0
<b>Target:</b>	HD 206893 (no det)				5/32/10 s	-72/6
<b>Target:</b>	HD 206893 (no det)				5/32/10 s	-70/-20
<b>Target:</b>	HD 206893 c				5/32/10 s	-55/-50
2021-09-28	01:13:14 / 03:53:59	1.00–1.15	3.9–3.4	0.8–1.2		
<b>Target:</b>	HD 206893 A				10/64/1 s	0/0
<b>Target:</b>	HD 206893 c				11/32/10 s	-76/-82
<b>Target:</b>	HD 206893 (no det)				8/12/30 s	-65/-30
2021-10-16	23:41:45 / 03:07:57	1.00–1.22	1.6–3.3	0.4–0.6		
<b>Target:</b>	HD 206893 A				12/64/1 s	0/0
<b>Target:</b>	HD 206893 c				27/32/10 s	-76/-82

**Table A.1.** Observing log of the four nights. NEXP, NDIT, and DIT denote the number of exposures, the number of detector integrations per exposure, and the detector integration time, respectively.  $\tau_0$  denotes the atmospheric coherence time. The values  $\Delta$ RA/ $\Delta$ DEC are the placement of the science fiber relative to the fringe tracking fiber (which is always on the central star).

capture or phase protection to play a role in the shaping or the stability of the companions orbits.

If the orbital configuration looks very similar at first to the  $\beta$  Pictoris system, the dynamics of the HD 206893 system is much closer to instability. This is due to the smaller separation between the two companions, and the higher mass and eccentricity of the inner companion. We sample randomly 1000 orbital solutions from the orbital fit, and perform  $N$ -body simulations starting from these solutions and lasting for  $10^5$  years. The simulations are performed using the Mercurius integrator in the Rebound package (Rein & Liu 2012; Rein et al. 2019), with a

time-step of 0.1 yr. We monitor the eccentricities of both companions and stop the simulations if one of them reaches one. The results are displayed on Fig. D.2: the simulations exclude  $e_b > 0.15$  and  $a_b < 9.5$  au, and they disfavor the highest masses. Extending the integration to  $10^6$  yr does not significantly change the results, so that we can assume the stable configurations remain stable for longer than the integration time. The probability that we are observing the system within  $10^5$  yr of a companion's ejection is very unlikely given its age, therefore the system is likely long-term stable. Despite the relatively large mutual separation, the system can be considered compact, as the orbits of the

Epoch [MJD]	$\Delta$ RA [mas]	$\sigma_{\Delta$ RA [mas]	$\Delta$ Dec [mas]	$\sigma_{\Delta$ Dec [mas]	$\rho$
<b>HD 206893 B</b>					
58681.40*	130.73	0.04	198.10	0.06	-0.58
58708.16*	127.03	0.09	199.27	0.13	-0.88
59453.10	20.08	0.08	205.81	0.11	-0.92
<b>HD 206893 c</b>					
59454.13	-76.31	0.21	-82.84	0.09	-0.92
59485.11	-72.11	0.08	-85.32	0.14	-0.87
59504.06	-69.33	0.05	-86.72	0.07	-0.61

**Table A.2.** GRAVITY astrometry of HD 206893 B and HD 206893 c. The astrometry with  $\star$  are already published astrometry from Kammerer et al. (2021). The co-variance matrix can be reconstructed using  $\sigma_{\Delta$ RA<sup>2</sup> and  $\sigma_{\Delta$ Dec<sup>2</sup> on the diagonal, and  $\rho \times \sigma_{\Delta$ RA  $\times$   $\sigma_{\Delta$ Dec on the off-diagonal.

Orbital Element	Prior	Posterior
$a_B$ (au)	LogUniform(1, 100)	$9.7^{+0.4}_{-0.3}$
$e_B$	Uniform(0, 1)	$0.14^{+0.05}_{-0.05}$
$i_B$ ( $^\circ$ )	$\sin(i)$	$146.2^{+3.3}_{-3.1}$
$\omega_B$ ( $^\circ$ )	Uniform(0, $2\pi$ )	$184^{+11}_{-11}$
$\Omega_B$ ( $^\circ$ )	Uniform(0, $2\pi$ )	$73.3^{+4.9}_{-3.1}$
$\tau_B$	Uniform(0, 1)	$0.310^{+0.035}_{-0.021}$
$a_c$ (au)	LogUniform(1, 100)	$3.53^{+0.08}_{-0.07}$
$e_c$	Uniform(0, 1)	$0.41^{+0.03}_{-0.03}$
$i_c$ ( $^\circ$ )	$\sin(i)$	$150.4^{+2.9}_{-3.1}$
$\omega_c$ ( $^\circ$ )	Uniform(0, $2\pi$ )	$46^{+8}_{-7}$
$\Omega_c$ ( $^\circ$ )	Uniform(0, $2\pi$ )	$89.4^{+6.9}_{-6.7}$
$\tau_c$	Uniform(0, 1)	$0.687^{+0.013}_{-0.010}$
Parallax (mas)	$\mathcal{N}(24.59, 0.26)$	$24.64^{+0.24}_{-0.24}$
$\gamma_{RV}$ (m/s)	Uniform(-5000, 5000)	$140^{+11}_{-12}$
$\sigma_{RV}$ (m/s)	LogUniform(0.1, 100)	$38^{+3}_{-3}$
$M_B$ ( $M_{Jup}$ )	Uniform(1, 50)	$27.4^{+2.3}_{-2.2}$
$M_c$ ( $M_{Jup}$ )	Uniform(1, 50)	$12.3^{+1.1}_{-1.2}$
$M_*$ ( $M_\odot$ )	$\mathcal{N}(1.29, 0.10)$	$1.32^{+0.07}_{-0.06}$
Derived Parameters		
$P_B$ (years)	-	$25.8^{+1.1}_{-1.2}$
$P_c$ (years)	-	$5.74^{+0.12}_{-0.11}$
Mutual Inc. ( $^\circ$ )	-	$9.6^{+5.5}_{-5.1}$

**Table B.1.** Full set of fitted orbital parameters for HD 206893 B and c, with some derived parameters included.

companions are close to instability. It suggests that ejection may be a likely outcome of the formation of two massive companions in planetary-like orbits.

Another important characteristic of this hierarchical three-body system is its relative coplanarity. Table B.1 shows indeed that the mutual inclination between both orbital planes is  $\sim 15^\circ$  at most. This actually reinforces the similarity with the  $\beta$  Pictoris system. This is also low enough to keep this system far enough from Kozai-Lidov resonance (Kozai 1962). That dynamical mechanism typically concerns nested orbits of different sizes having a sufficient enough mutual inclination ( $\gtrsim 39^\circ$  theoretically). When this occurs, the inner orbit is subject to large amplitude eccentricity oscillations that can drive it to very high values close to unity. This can lead to direct instability or to a potential collision with the central star due to a decaying periastron. The latter fate can be prevented by tides within the inner orbit, but even in that case, the orbit does not remain as it is and furthermore shrinks significantly (Fabrycky & Tremaine 2007; Beust et al. 2012). The mutual inclination determination (Table B.1) shows that there is no risk of Kozai-Lidov resonance

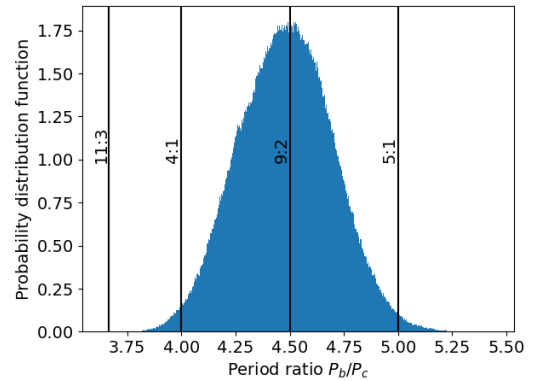


**Fig. D.1.** Probability distribution of of HD 206893  $b$  and  $c$  period ratios from the orbital fit.

here, which reinforces the likely stability of the system. This also favours the stability of the debris disk, as disk particles could be affected by Kozai-Lidov mechanism as well.

Finally, we note that the stable configurations are just snapshots of a system with complex and evolving dynamics. We use the approach described in Lacour et al. (2021) to estimate the secular eccentricity variation and the associated period. We exclude solutions with  $e_b > 0.15$  and  $a_b < 9.5$  au to ensure stability. The results are displayed on Fig. D.3. The eccentricity of  $b$  can periodically vanish, while  $e_c$  can reach values as high as 0.5. These variations are expected to occur over timescales of  $\sim 10^4$  yr. This is important to keep in mind when discussing the formation of the orbital architecture (as it could have formed at any point of the secular cycle), or the impact of the companions on the other components of the system (debris disk, additional planets...).

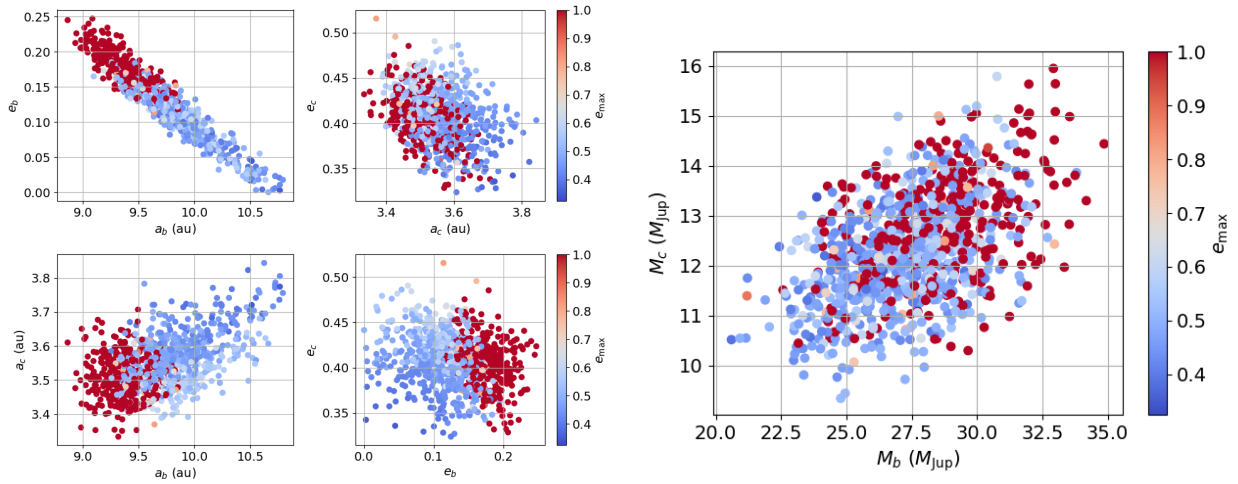


**Fig. D.2.** Maximum eccentricity reached by either companion in  $N$ -body simulations with initial conditions representative of the orbital solutions. The simulations are performed for  $10^5$  yr using the Mercurius integrator.

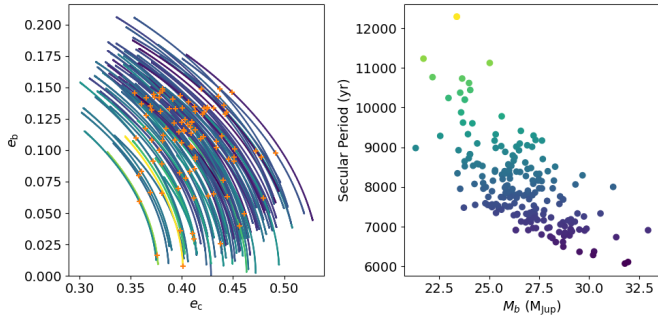


**Fig. D.3.** Secular evolution of the eccentricities of  $b$  and  $c$  due to their mutual interaction. Left is the trajectory in  $(e_b, e_c)$  phase space, starting from the observed values (orange crosses, which are random solutions to the orbital fit using all available data). We exclude the initial conditions with  $e_b > 0.15$  and  $a_b < 9.5$  au, as discussed above. The colours represent the corresponding eccentricity evolution period (secular period). The right panel represents the aforementioned period with respect to the mass of  $b$ .